Numerical Simulation of Cryogenic Injection in Rocket Engine Combustion Chambers

P. Gaillard, C. Le Touze, L. Matuszewski, A. Murrone

▶ **To cite this version:**

P. Gaillard, C. Le Touze, L. Matuszewski, A. Murrone. Numerical Simulation of Cryogenic Injection in Rocket Engine Combustion Chambers. Aerospace Lab, 2016, 11, pp.16. 10.12762/2016.AL11.16 . hal-01369627

HAL Id: hal-01369627
https://hal.science/hal-01369627v1

Submitted on 21 Sep 2016

HAL is a multi-disciplinary open access archive for the deposit and dissemination of scientific research documents, whether they are published or not. The documents may come from teaching and research institutions in France or abroad, or from public or private research centers.

L'archive ouverte pluridisciplinaire **HAL**, est destinée au dépôt et à la diffusion de documents scientifiques de niveau recherche, publiés ou non, émanant des établissements d'enseignement et de recherche français ou étrangers, des laboratoires publics ou privés.

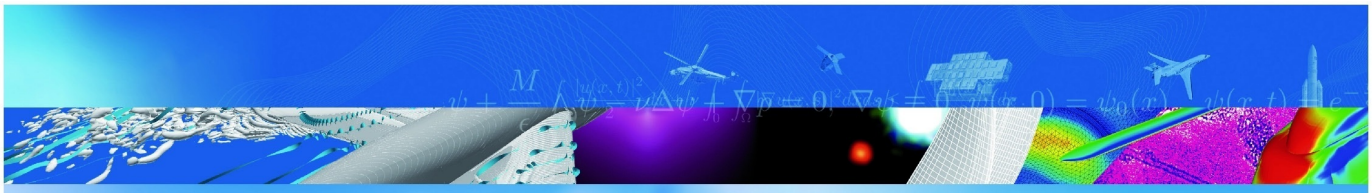

ARTICLE DE REVUE

Numerical Simulation of Cryogenic Injection in Rocket Engine Combustion Chambers

P. Gaillard, C. Le Touze,
L. Matuszewski, A. Murrone

AEROSPACELAB JOURNAL

No 11, AL11-16, 11 pages

TP 2016-560

70 2016 ans

ONERA

THE FRENCH AEROSPACE LAB

P. Gaillard, C. Le Touze, L. Matuszewski, A. Murrone
(ONERA)

E-mail: lionel.matuszewski@onera.fr

DOI : 10.12762/2016.AL11.16

Numerical Simulation of Cryogenic Injection in Rocket Engine Combustion Chambers

The numerical simulation of cryogenic combustion is crucial for a better understanding of the complex physics involved in reactive flows of rocket engines and to help to reduce the development cost of these engines. The focus of this study is set on the oxidizer injection and its dispersion through jet dense core destabilization and atomization or supercritical mixing. Specific models have been implemented in the CFD code CEDRE created by ONERA to address these physical phenomena.

Introduction

In the field of chemical rocket propulsion, oxygen and hydrogen are favored over other types of fuel due to the high specific impulse (Isp) that they produce. This Isp represents the ratio between the thrust (in mass equivalent units) and the fuel consumption, so that the higher the Isp, the heavier the payload can be. Oxygen and hydrogen can be easily obtained through air distillation and hydrocarbon cracking, but these components are gaseous at ordinary temperature. In order to minimize the rocket fuel tank structure, oxygen and hydrogen are liquefied at a very low temperature, hence leading to cryogenic combustion.

Such extreme conditions require specifically designed test benches, such as the MASCOTTE test bench [1], in order to provide an insight into the characteristic phenomena involved in cryogenic combustion.

To complement this experimental approach, numerical simulations with the CEDRE [2] code are conducted on test-case configurations, in order to develop numerical tools and models with the ultimate aim being predictable numerical simulation, which would make the designing of industrial scale rocket engines easier.

This paper focuses on oxidizer dispersion through dense core destabilization, which leads to small scale structures eventually breaking into droplets or dense clusters, depending on the chamber pressure. This dispersion of oxygen greatly influences the flame shape and thus the overall combustion process, but is still difficult to represent numerically since it involves very different large scales.

Subcritical regime and atomization

Two-phase flows resulting from the atomization of liquid jets play a significant role in the proper functioning of cryogenic liquid-propellant rocket engines under subcritical operating conditions [3]. As depicted in figure 1, the great velocity difference between the two phases (liquid Ox and Gaseous H_2) at the exit of a coaxial cryogenic injector generates fluctuating accelerations. Due to these fluctuations, Rayleigh-Taylor instabilities destabilize the liquid to create ligaments. These instabilities then grow and eventually cause the peeling of the main LOx jet, which is referred to as "primary atomization". Large random-shaped liquid structures are thereby ejected towards the gas flow, subsequently undergoing "secondary break-up" when inertia forces exceed the liquid surface tension. This results in a spray of small LOx droplets, mainly spherical, which are dispersed by the turbulent gas flow and finally vaporized to feed the combustion with hydrogen. Such a configuration therefore exhibits a two-phase flow where the liquid phase is only composed of LOx, whereas the gas phase is made up of hydrogen H_2, vaporized oxygen O_2 and combustion products. Eventually, the resulting high-enthalpy combustion products exhaust through a nozzle at supersonic speed, thereby providing the required thrust.

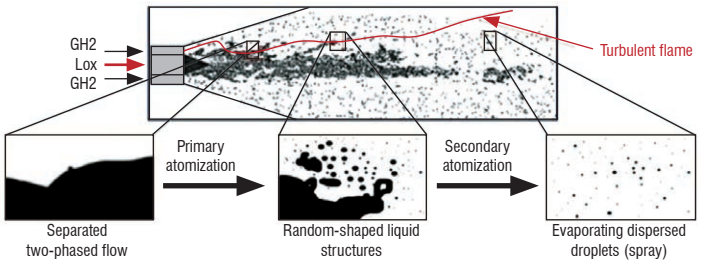

Figure 1 – Configuration of a combustion chamber within liquid-propellant rocket engines under subcritical operating conditions

Since the experimental investigation of such propulsion devices is complex and expensive, developing numerical tools able to accurately simulate their functioning, including all of the physical phenomena and their interactions, is a crucial but nonetheless ambitious objective. Indeed, the harsh conditions within cryogenic rocket engines, where great temperature, velocity and density gradients are encountered, severely challenge the robustness of numerical methods. Another major difficulty is due to the multiscale nature of the problem.

A large amount of models is available in the literature for the numerical simulation of multiphase flows. These range from interface tracking methods (Level Set, Volume of Fluid) to diffuse interface methods with potentially different levels of physical modeling (from the 7-equation model to the 4-equation model), and to kinetic (statistical) models for dispersed phases. The problem is that if the simulation of a whole combustion chamber is sought, even in a simplified single-injector configuration such as the MASCOTTE bench, any mesh that would be refined enough to capture the smallest droplets with any of the interface tracking methods is still absolutely unattainable. With diffuse interface methods, it is possible to describe the liquid phase in a continuous way, from injection to primary and secondary atomization and vaporization. For instance, primary atomization can be described as a source term based on a transport equation for the surface area density [4]. However, sprays are best described by dedicated statistical models based upon either a Lagrangian or Eulerian formalism, in which local polydispersity can be taken into account. Unfortunately, there is no straightforward coupling between diffuse interface models (or interface tracking models) and statistical models, which would be interesting for predictive simulations of reactive flows including primary atomization.

Based on this observation, the work presented here is aimed at setting up a coupling strategy between different models, each one being suitable for a specific two-phase flow topology. The approach adopted specifically consists, within the scope of the multiphysics CEDRE software developed at ONERA, in coupling:

- a model suitable for the "separated" and "mixed" areas of the two-phase flow (see figure 1), based on a diffuse interface approach and a locally homogeneous flow assumption ("4-equation" model), in a LES context and resolved by the CHARME solver of CEDRE,
- and a Eulerian kinetic model for the dispersed phase, based on a sectional method to describe the droplet size distribution and resolved by the SPIREE solver of CEDRE.

Note that similar strategies have been developed in the literature. However, most of them are based on a RANS formulation and a Lagrangian formalism when coupling with the dispersed phase (see [5] and related works), whereas this work is aimed at Large Eddy Simulation and uses a fully Eulerian formalism.

In order to achieve this goal, we have developed a coupling model between the CHARME and SPIREE solvers of CEDRE, intended to account for primary atomization. In the following we first further explain our strategy for the simulation of primary atomization applied to subcritical cryogenic combustion: what has been done so far and what remains to be done in future works. Then, we briefly present the details of the equations resolved by each solver, give a few details on source term expression and numerical methods (further details on these topics can be found in [3] and [8]), and introduce the primary atomization model. We finally present some first numerical results of a Large Eddy Simulation using the proposed strategy. This simulation has been performed on the MASCOTTE test bench configuration, specifically on the 10-bar operating point corresponding to cryogenic rocket engines under subcritical operating conditions. Eventually, it should be stressed that this is still a work in progress and more advanced simulation results on the MASCOTTE configuration are to be presented in future communications.

Description of the coupling strategy

Figure 2 illustrates the coupling strategy between the CHARME and SPIREE solvers. In this figure, the subscripts "CH" and "SP" respectively stand for CHARME and SPIREE, the color red indicates the gas phase and the color blue represents the liquid phase. The green dashed lines illustrate the coupling between CHARME and SPIREE. This is obviously a schematic representation: in reality the phenomena are not fully decoupled and sequential. On the contrary, there exists a large area where atomization, secondary break-up, evaporation and even combustion in gaseous phase occur almost simultaneously. Besides, it is important to specify that both solvers share exactly the same computation domain (and the same mesh as well). Thus, the SPIREE solver deals with the entire geometry and is not restricted to a pre-defined area, even though there are obviously large zones of the geometry where the dispersed phase is never encountered. Note that in these no-droplet areas the computational cost of SPIREE is reduced to almost zero. Hence, the sub-domain decomposition of the computation domain must be performed carefully so as to reach an optimal overall load balancing.

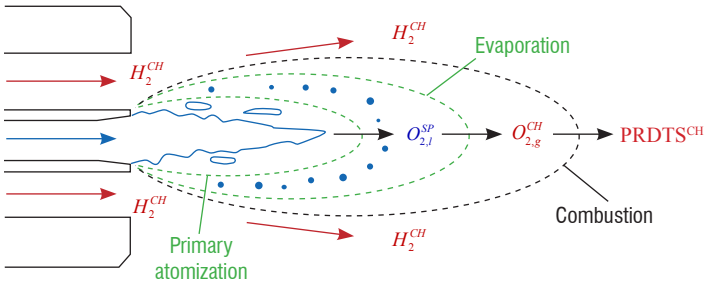

Figure 2 – Coupling strategy between the CHARME and SPIREE solvers

Going into more details, the strategy as illustrated in figure 2 is as follows:

- The CHARME solver performs the Large Eddy Simulation of the two-phase fluid, which gathers a turbulent reactive gaseous phase made up of multiple chemical species (including oxygen, hydrogen and combustion products) and a liquid phase made up of only one species: the LOx. The description of the liquid phase with CHARME is restricted to the "separated" and "mixed" areas of the two-phase-flow, which are precisely the dense liquid core and the mixture zone downstream the injector exit, where the liquid jet is sheared by the co-axial high velocity gaseous flow. The mesh is designed so as to be refined enough to describe the instabilities at the surface of the liquid core and even the formation of some ligaments.
- It is impossible to pursue this strategy up to the description of the droplets, given that any mesh that would be refined enough for that would be absolutely unattainable for practical applications. In other words, the droplet generation is inevitably a phenomenon that must be addressed at the sub-grid scale level. This is the reason why we operate a transfer from CHARME to SPIREE, so that the droplets can be described with a dedicated model. Under the effect of a source term based on some local criteria (see the following sections), the LOx mass (as well as the associated momentum and energy) is withdrawn from the CHARME solver, in the "mixed" two-phase flow area, and transferred to the SPIREE solver. When in SPIREE, the LOx mass is assumed to be in the form of purely spherical dispersed droplets.

• Then, the droplets are transported within the SPIREE solver, in which they break-up and vaporize. The latter is a reverse transfer towards the CHARME solver: the mass of liquid oxygen droplets is transferred to the gaseous oxygen species in the CHARME solver. Note that vaporization is only taken into account in this way, namely when LOx is in the form of droplets. It could be also possible to include a vaporization term within the CHARME solver, so as to describe the LOx vaporization prior to droplet formation. This would therefore be an "intern" source term in the CHARME solver, describing a transfer between both liquid and gaseous oxygen species. This point has not been considered for now.

• Finally, the chemical reaction between the gaseous oxygen coming from the droplet vaporization and hydrogen (turbulent diffusion flame) is described within the CHARME solver through dedicated source terms.

Note that the strategy still needs to be enhanced for a better description of the "mixed" zone. For instance, the use of a transport equation for the surface density area (adapted to the LES context) should improve the description of the sub-grid dispersion of the liquid phase, thereby enabling a more continuous and accurate description of the transition from the "mixed" topology (ligaments, non-spherical large "droplets", etc.) to the spray generation. Note however that this point is obviously of lesser importance here, in a LES context, than it would be within a RANS framework. Besides, let us add the following comments:

• The coupling between CHARME and SPIREE is only through source terms (the volume fraction of the dispersed phase is assumed to be negligible and therefore not taken into account in CHARME) and is fully conservative in mass, momentum and energy. Coupling source terms describe mass, momentum and energy transfers respectively, because of primary atomization (transfer from the liquid phase of the fluid towards the dispersed phase) and vaporization (transfer from the dispersed phase towards the gaseous phase of the fluid), drag force and heat flux. Each solver has also "intern" source terms, to describe combustion in the case of CHARME and to describe secondary fragmentation in the case of SPIREE.

• Using the Eulerian formalism rather than the Lagrangian one for the dispersed phase seems more natural, convenient and effective when setting up the kind of coupling strategy presented here. Indeed this facilitates a conservative and robust coupling (see [8] for further discussion on this issue).

In the following two sections, the equations of the models used for both "separated" (CHARME solver) and "dispersed" (SPIREE) two-phase-flow are presented.

Diffuse interface model for the "separated" two-phase flow (CHARME)

The system resolved by the CHARME solver is a so-called "4 equation" diffuse interface model, based on a locally homogeneous flow assumption. This is nothing other than the multi-species compressible Navier-Stokes system, where we consider a fluid mixture composed by one gaseous phase of ng species and one liquid phase made up of only one species, which is the dense LOx. The classical Navier-Stokes system in vectorial form is written as:

$$\frac{\partial \mathbf{Q}(\mathbf{U})}{\partial t} + \nabla \bullet \left[F_c(\mathbf{U}) - F(\mathbf{U}, \nabla \mathbf{U}) \right] = S(\mathbf{U})$$

In this system, conservative and primitive sets of variables respectively are written as:

$$\mathbf{Q}(\mathbf{U}) = \left(\rho Y_1 \quad \dots \quad \rho Y_{n_g} \quad \rho Y_l \quad \rho \mathbf{v} \quad \rho e_{tot} \right)^t$$

$$\mathbf{U}(\mathbf{Q}) = \left(P \quad T \quad \mathbf{v} \quad Y_1 \quad \dots \quad Y_{n_g} \quad Y_l \right)^t$$

where $Y_i \quad i = 1, \dots, n_g$ stand for the mass fractions of gaseous species while Y_l stands for the mass fraction of the dense LOx. Thus, ρ is the mixture density, e_{tot} is the total energy and P, $\mathbf{v}$, T respectively stand for the local unique pressure, velocity vector and temperature of the whole fluid. The convective and diffusive fluxes can be written in the form:

$$F_c(\mathbf{U}) = \mathbf{Q} \otimes \mathbf{v} + P \left(0 \quad \dots \quad 0 \quad \mathbf{I}_3 \quad \mathbf{v} \right)^t$$

$$F(\mathbf{U}, \nabla \mathbf{U}) = \left(F_{\rho Y_1} \quad \dots \quad F_{\rho Y_{n_g}} \quad F_{\rho Y_l} \quad F_v \quad F_e \right)^t$$

Let us give the following important detail: in this work we do not include any subgrid-scale turbulence modeling and therefore only consider an implicit approach for LES. Accurate modeling of subgrid-scale dissipation in a compressible two-phase flow context and on general heterogeneous unstructured meshes is a complex issue, which will be addressed in future works. Therefore, the diffusive fluxes only gather here the classical laminar diffusion terms: the molecular species diffusion in the gas phase described by Fick's law, the viscous stress tensor and Fourier's law for heat conduction. Finally, the source term vector $S(\mathbf{U})$ includes combustion modeling and coupling source terms between the CHARME and SPIREE solvers (see details in the following sections).

Eulerian kinetic-based model for the dispersed phase (SPIREE)

At the highest level of precision, the modeling of dispersed two-phase flows is based on a mesoscopic description provided by the Williams-Boltzmann kinetic equation. Particles are assumed to be spherical and fully characterized by a small set of variables: position $\mathbf{x}$, radius r, velocity $\mathbf{v}$ and temperature θ. The following Boltzmann-like equation expresses the conservation of the number density function (n.d.f) $f(t, \mathbf{x}, r, \mathbf{v}, \theta)$ in the phase space:

$$\frac{\partial f}{\partial t} + \nabla_{\mathbf{x}} . (\mathbf{v} f) + \nabla_{\mathbf{v}} . (\mathbf{F} f) + \frac{\partial}{\partial r}(R f) + \frac{\partial}{\partial \theta}(H f) = \Gamma + Q$$

In this balance equation, the left-hand-side stands for the "transport" of the particles in the phase space ($\mathbf{F}$, R and H respectively correspond to the force acting on a particle, the evaporation rate and the heat exchange rate), while Γ, Q on the right-hand-side respectively stand for the effect of fragmentation and collision phenomena. Note that $\mathbf{F}$, R and H depend on the local gas composition, velocity and temperature.

All fluid models for gas-particle flows are based on conservation equations for some particular moments of the number density function. These models can be formally derived from the kinetic equation by particular closure assumptions. The details of this derivation are not reproduced here (see for instance [6], [7], [8]). Only note that the choice of the discretization strategy for the size variable is of utmost importance, since we want to precisely describe the polydispersity of the spray. This is why we opt for the sectional approach, which is illustrated in figure 3. Information regarding the droplet size distribution

is kept at the macroscopic level thanks to a finite volume discretization with respect to the size variable. A set of equations is derived for each section and, in this type of model, sections are coupled thanks to mass, momentum and heat fluxes. More complex phenomena such as coalescence and fragmentation can also be easily included. Here we only consider the fragmentation term Γ.

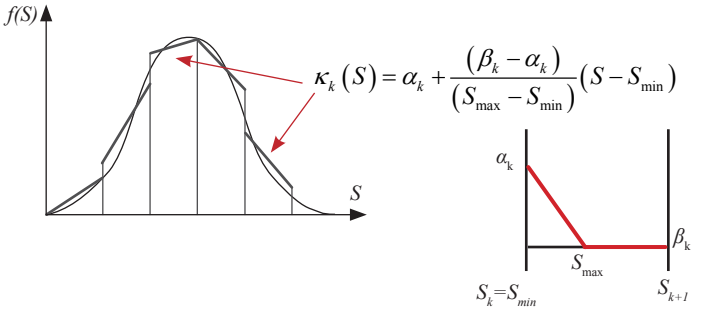

Figure 3 – Sectional approach with piecewise linear function reconstruction

Compared to other reconstructions, the main advantages of the linear function reconstruction are the positivity conservation when computing the inversion between the moments (mass and number density) and the reconstruction coefficients (α_k, β_k, s_{min}, s_{max}), and the computational cost reduction [7]. When using this reconstruction, we also maintain the possibility of performing the exact computation of the integrated source terms. Finally, the system of equations resolved by the SPIREE solver for each section of the dispersed phase is written as:

$$\frac{\partial \mathbf{q}(\mathbf{u})}{\partial t} + \nabla \bullet \left[f_c(\mathbf{u}) \right] s(\mathbf{u}) + \Gamma \text{ where } f_c(\mathbf{u}) = \mathbf{q} \otimes \mathbf{v}_d$$

The conservative and primitive variables are:

$$\mathbf{q}(\mathbf{u}) = \left(\rho_d \quad \rho_d \mathbf{v}_d \quad \rho_d h_d \quad N_d \right)$$
$$\mathbf{u} = \left(D \quad \mathbf{v}_d \quad T_d \quad \alpha \right)$$

In this system, $\rho_d = \alpha \rho_0$ stands for the bulk density of particles (ρ_0 is the density of pure liquid), N_d for the average number of particles per unit of volume and h_d for the total energy. The primitive variables D, $\mathbf{v}_d$, T_d, α are respectively the mean particle diameter, the velocity vector, the temperature and the volume fraction. The source terms vector $s(\mathbf{u})$ gathers the classical source terms between the gas phase in the CHARME solver and the dispersed phase (drag force, heat and mass transfer), as well as the new source term specifically designed to describe the coupling between the liquid phase in the CHARME solver and the dispersed phase (primary atomization). The secondary break-up vector Γ comprises source terms between the size sections: the break-up of large droplets into smaller droplets results in a mass, momentum and energy transfer between the various sections.

Source term expression and numerical methods

Let us now describe the components of the source term vectors $s(\mathbf{u})$ and $S(\mathbf{u})$, concerning respectively each section of particles in the SPIREE solver and the CHARME solver. The first component in s(u) represents, for a given section, the increase in the droplet mass due to primary atomization and its decrease by vaporization. In the second component (momentum), we find the effect of the drag force. The third component (total energy) includes the power of the drag force and the heat flux. Finally, the last component for the number density comprises a term corresponding to the new droplets that are created by primary atomization. If we now look at the source term $S(\mathbf{u})$ assigned to the carrier phase CHARME, the first n_g components (gas species) include combustion terms (the reaction rates are obviously zero for inert species). If we assume that the first species is the gaseous oxygen, then the first term also includes the evaporation of liquid oxygen droplets. The component number n_g+1 is for the liquid species and therefore includes the primary atomization source term. It transfers the dense LOx of CHARME into "dispersed" LOx in the appropriate sections of SPIREE.

$$s(\mathbf{u}) = \begin{pmatrix} s_{\rho_d} \\ s_{\rho_d \mathbf{v}_d} \\ s_{\rho_d h_d} \\ s_{N_d} \end{pmatrix} = \begin{pmatrix} \dot{M}_{ato} - N_d \dot{m}_{vap} \\ s_{\rho_d} \mathbf{v}_d + N_d \mathbf{F}_D \\ s_{\rho_d} h_d + N_d \left(\mathbf{F}_D . \mathbf{v}_d + \varphi_c \right) \\ \dot{N}_{ato} \end{pmatrix} \quad S(\mathbf{U}) = \begin{pmatrix} \dot{w}_{O_2} + N_d \dot{m}_{vap} \\ \dot{w}_i \\ \vdots \\ \dot{w}_{n_g} \\ -\dot{M}_{ato} \\ -s_{\rho_d \mathbf{v}_d} \\ -s_{\rho_d h_d} \end{pmatrix}$$

Classical coupling source terms between the gas phase and the dispersed phase

The evaporation and heat transfer modeling ($\dot{m}_{vap}$ and ϕ_c) is based on the classical Abramzon-Sirignano model [9] and the drag force $\mathbf{F}_D$ is modeled using the Schiller-Naumann correlation. Details on these models can be found in [8].

Fragmentation source terms

The expression of the fragmentation source terms vector Γ is based on:

- a model for the break-up of an isolated droplet, whose expression can be found in the literature (see [10] for instance),
- a numerical integration procedure in order to turn this model at the droplet scale into a mean fragmentation operator Γ (see [11]).

More details on these points can be found in [8] and in the above-mentioned references.

Turbulent Combustion

The H_2-O_2 combustion is modeled using an infinitely fast chemistry assumption (high Damkohler number). This means that kinetic effects are not taken into account. The species production rates are related to the gap between the local and equilibrium concentrations, respectively Y_i and $Y_{i,eq}$. In other words, the reacting species are relaxed towards chemical equilibrium with a finite relaxation time driven by a turbulent time scale ν_{turb}^{-1}. In the LES framework, such a time scale can be assumed from the resolved strain tensor. This approach is similar to the well-known “Eddy Break-Up” model, since in both approaches infinitely fast chemistry is assumed. Fortunately however, taking into account a local equilibrium involving radical species renders a much more accurate flame temperature. The reaction rate is then written as:

$$\dot{w}_i = ctev_{turb} \left(Y_{i,eq} - Y_i \right)$$

Numerical methods

The numerical methods used in this work are based on a Finite Volume approach for general unstructured meshes, for both the CHARME and

SPIREE solvers. Given that the coupling between these two solvers includes a large variety of phenomena, we use a time splitting technique whose details can be found in [3]. Concerning spatial approximation, we have developed a new second-order multislope MUSCL technique for general unstructured meshes [12], in order to ensure the robustness of the simulation. We also use upwind schemes, such as the classical HLLC scheme for the CHARME solver and a Godunov-like scheme for SPIREE adapted to the weak hyperbolicity of the system of particles (equivalent to the system of pressureless gas dynamics).

Primary atomization modeling

The model developed to describe the mass transfer between solvers accounting for primary atomization is written as:

$$\dot{M}_{ato} = \rho Y_l \nu_{ato} \lambda_{ato}(Y_l)$$

where ρY_l is the liquid mass in a given control volume, ν_{ato} is the characteristic frequency of the primary atomization process and $\lambda_{ato}(Y_l)$ is an efficiency function. We assume the atomization frequency to be directly connected to the strength of the velocity gradient, which is the only information locally available in the 4-equation framework (no velocity difference is known). This could be estimated using several approaches, amongst which are the Q criterion, the vorticity or the resolved strain tensor, all of these being based on the velocity gradient. In this study we have chosen to use the latter approach:

$$\nu_{turb} = \sqrt{2D^2} \quad ; \quad D^2 = \sum_{ij} D_{ij} D_{ij} \quad ; \quad D_{ij} = \frac{1}{2}\left(\frac{\partial \bar{u}_i}{\partial x_j} + \frac{\partial \bar{u}_j}{\partial x_i} \right)$$

The efficiency function is written as:

$$\lambda_{ato}(Y_l) = 1 - \tanh(a_\lambda Y_l^{b_\lambda}) \quad a_\lambda = 4, \quad b_\lambda = 2$$

It is designed to ensure that when some LOx mass is transferred from the fluid towards the spray in a given control volume, the corresponding vanishing volume in the fluid is actually negligible. Otherwise, the gas would experience some unphysical expansion in the control volume, which obviously has to be avoided, and the dispersed phase hypothesis made for the spray would not be respected. In other words, we use the numerical diffusion, which spreads the interface over several mesh elements, in order to carry out the mass transfer in a smooth way.

At this point with this model, the properties of the created droplets resulting from the primary atomization have to be assumed. They cannot be computed locally from resolved quantities, since the 4-equation formalism provides too little information. Actually, these properties are estimated based on the instability analysis from the reference [13]. In the latter work, the drop size and velocity distributions of the spray are estimated as a function of the injected propellant properties (density ratio, inlet velocities, vorticity thickness, etc.). Consequently, the knowledge of the steady operating conditions of the MASCOTTE configuration enables an overall mean droplet diameter subsequent to the primary atomization process to be derived and a corresponding mean droplet velocity:

$$d_{ato} = 260\mu m, \quad \|v_{ato}\| = 16 m s^{-1}$$

The direction given to the droplet velocity in each mesh cell has been set to that of the fluid, which may be actually a rough approximation. Note that even if the created droplet diameter is assumed, the use of a secondary break-up model is expected to rapidly modify and somehow correct the local droplet diameter. In fact, the zone of secondary atomization is expected to be correctly computed. Concerning the zone of primary atomization, the computation is limited by the 4-equation model, in which only one velocity is available. Finally, the temperature of the created droplet is just set to the constant value that was used to describe the liquid phase in the fluid, namely 85 K, corresponding to the LOx injection temperature.

It should also be stressed that the primary atomization model, which describes only the transfer from the separated phase CHARME solver to the dispersed phase solver SPIREE, can be combined with another model describing the inverse liquid-liquid transfer, namely from the SPIREE solver to the CHARME solver. This term is intended to describe, for instance, the case of droplets impacting the main liquid jet. Details on this term are not provided here, but can be found in [8].

Finally, let us specify that, even if the created droplets all have the same size, the use of the sectional approach is completely relevant. Indeed, it allows us to describe the local size polydispersity, which is subsequent to primary atomization as droplets undergo secondary break-up and evaporation. Consequently, this improves the evaluation of the gas-particle source terms, since they all depend on the droplet size: vaporization, drag force and heat exchange. Also, the improvement of the primary atomization model is planned for future works, for instance by using a transport equation for the surface density area and/or by switching to a diffuse interface model giving more local information than the 4-equation model: a two-temperature (5-equation) model, or even a two-temperature two-velocity (7-equation) model. Therefore, this should enable us to predict distributions (size, velocity, etc.) for the droplets subsequent to primary atomization, rather than just assumed mean values, which will we be much easier in a sectional framework.

Numerical results

In this section, we present some numerical results obtained with the coupling strategy applied to the MASCOTTE bench configuration. The 3D geometry is depicted in figure 4. The overall device is approximately 50 cm long, with a 50 mm wide section. The LOx post has a 5 mm diameter, whereas the total diameter of the injector (axial LOx + coaxial H_2) is 12 mm. We use a tetrahedral unstructured mesh made up of approximately 9.8M elements. The mesh has been built so that the finest refinement is located near the injector exit, where atomization takes place. The smallest cell size is of the order of 100 μm (in the blue zone), whereas the maximum cell size is of the order of 3mm at the end of the chamber. Figure 4 also represents the mesh with a zoom near the injector. For the sake of simulation, the computational geometry has been split into 1920 sub-domains and then dispatched into 480 processors to allow parallel computing. The physical time step of the computation is about 2.10-8s. The total physical time computed is 17ms, which corresponds to a total CPU time of about one million hours. Numerical results are presented in the rest of the section. Comparisons with experimental results are only qualitative because the results are not yet converged, as illustrated in figure 5.

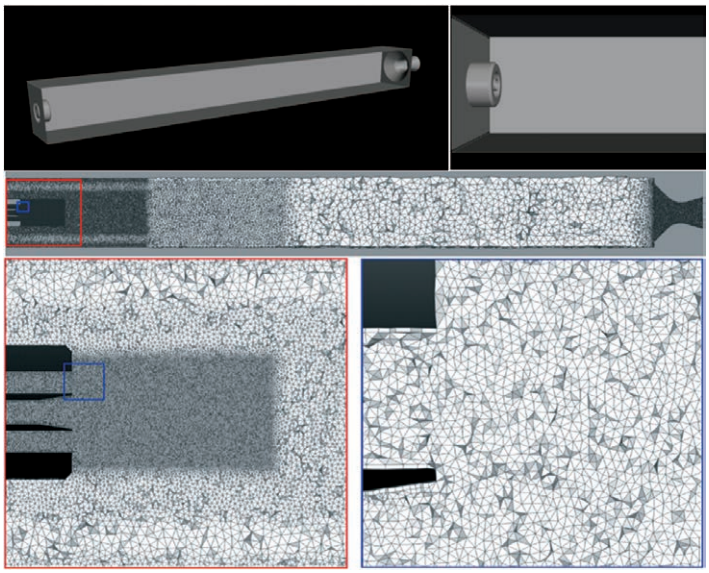

Figure 4 – Representation of the geometry and associated mesh for the MASCOTTE cryogenic test bench

Figure 5 shows the evolution of pressure and temperature obtained by the resolution of the CHARME solver, as well as the spray volume fractions obtained by the SPIREE solver (the volume fraction of each section is shown and the total one as well). Also shown is the evolution of the length of the liquid core over time. Results appear clearly not converged at this point of the computation because they include the end of the transient regime. The mean pressure decreases in the interval [0ms, 4ms] and reaches a minimum value equal to 7 bar. Then, the first droplets appear and feed the combustion, which induces an increase in the pressure. Between the times of 4 and 13 ms, the pressure increases to a maximum value equal to 10.7 bars and then decreases to reach 10.1 bars. In the experiments, the nominal pressure is equal to 11 bars. The maximum temperature can be related to the formation of the stable flame. A maximum value between 3500K and 3600K is obtained at 4 ms. Figure 5 also represents the evolution of the volume fraction for the three sections of the spray that are not empty. The volume fraction of the three sections globally increases with a total volume fraction that tends towards 0.02. Likewise, we can observe that the transient regime is not finished and that the LES "averaged" results have not converged. We have also plotted the length of the liquid core, which is evaluated in the simulation with the position of the isoline of the liquid volume fraction equal to 0.99. This length increases during the simulation as expected and seems to stabilize around a value between 11 and 13 mm. This length is approximately stable at 8 ms.

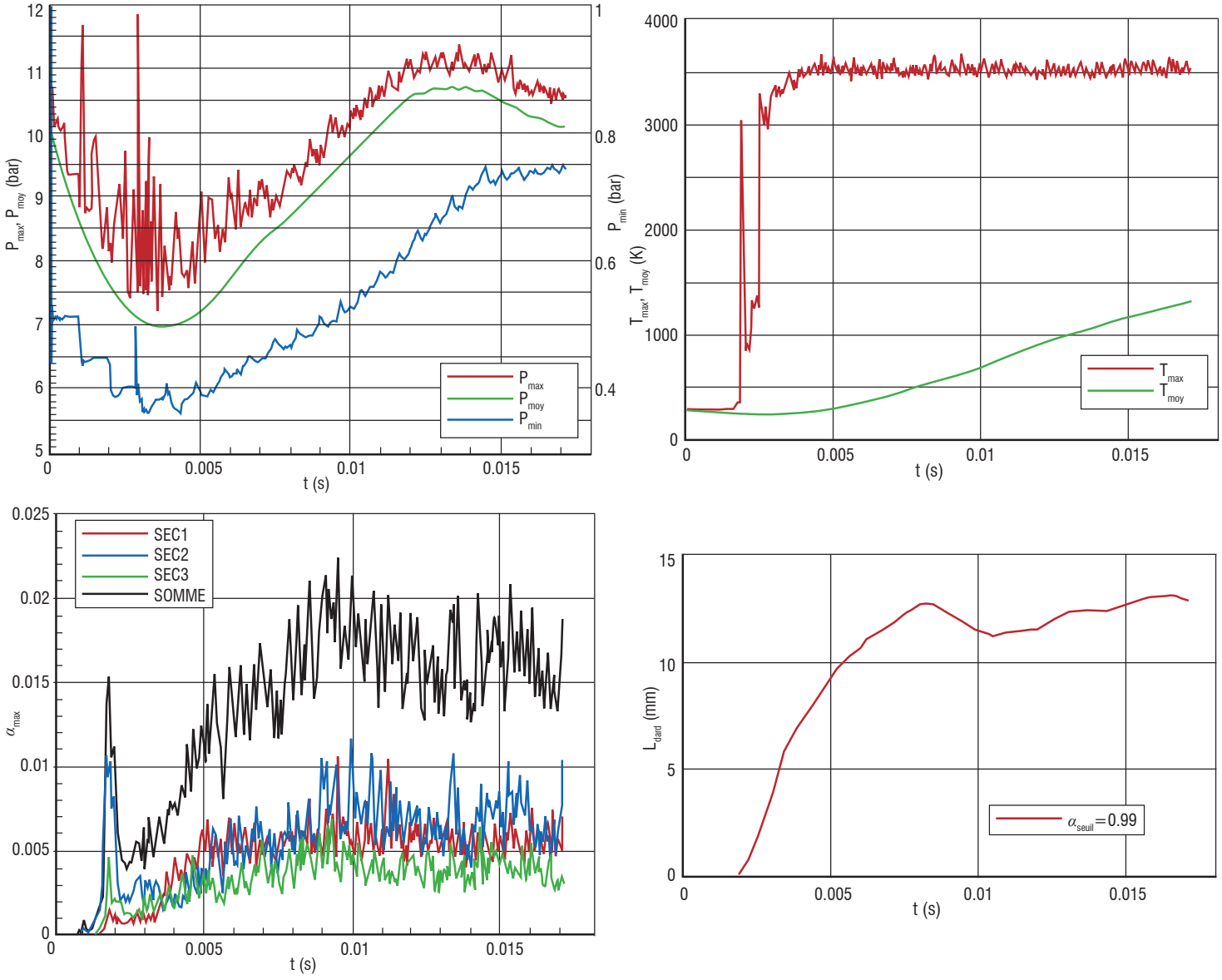

Figure 5 – Time evolution of pressure, temperature, volume fractions and penetration depth

The comparison with the theoretical value of 8 mm or experimental values between 8 and 41 mm is quite good, but must be confirmed with a higher level of convergence. In addition, the interpretation of the penetration depth must be made carefully because of numerical diffusion.

We then present different mean fields for the fluid solver in figure 6 to figure 10. The averaged field is computed between times 13 ms and 17 ms. Each variable is represented in the (XZ) plane and we have plotted the temperature and velocity isovalues, as well as the liquid and gaseous oxygen mass fraction and the H_2 gas and the H_2O product of combustion. The velocity norm is represented with logarithmic scaling. We can observe the recirculation of the coaxial H_2 with high velocity around the liquid oxygen, which has a low velocity and is atomized. In the lateral position, we can also observe the helium film, which is used in the experiment to cool the walls. A recirculation of H_2 is also observed. The mean value of the mass fraction clearly illustrates the transition region between separated and dispersed two-phase flow.

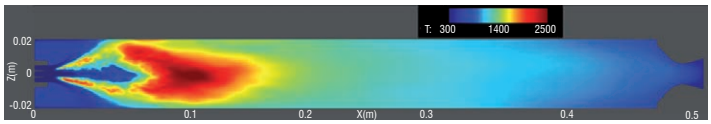

Figure 6 – Temperature mean field

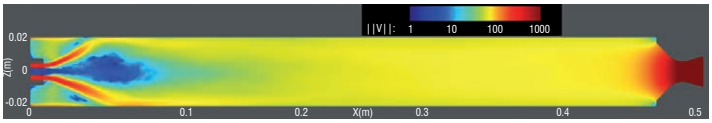

Figure 7 – Velocity norm mean field

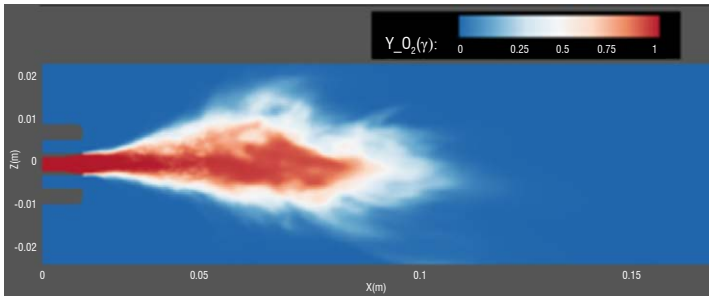

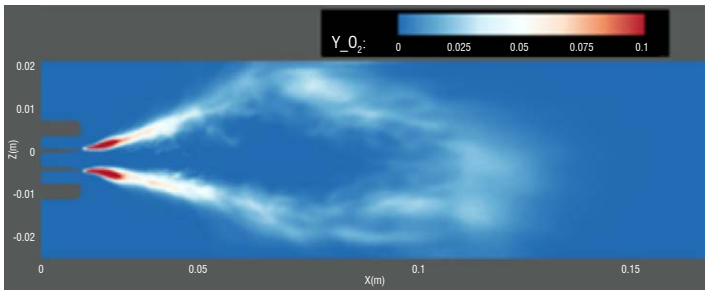

Figure 8 – Liquid oxygen (top) and gaseous oxygen (bottom) mass fraction mean field

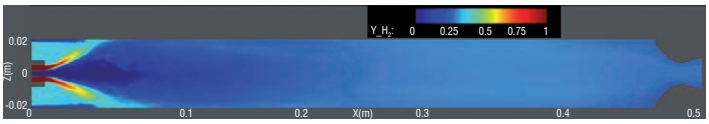

Figure 9 – Gaseous H_2 mass fraction mean field

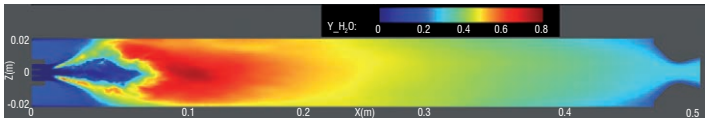

Figure 10 – Gaseous H_2O combustion product mean field

We also present on figure 11 instantaneous fields in the plane (XY) of both the total spray volume fraction (including all size sections), and the net liquid-liquid mass source term (labeled as ΔS_L in the key). The latter is the difference between the inverse liquid-liquid mass source term (re-impingement) and the primary atomization source term. Therefore negative values indicate zones where atomization takes place (mass is transferred from the continuous "separated phases" description to the "dispersed phase" description), whereas positive values indicate zones where the inverse transfer occurs.

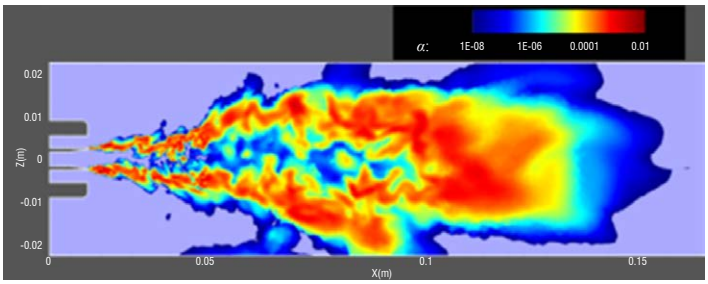

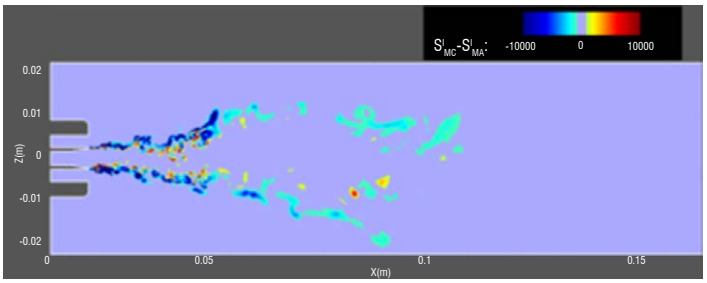

Figure 11 – Top: instantaneous field of the total spray volume fraction (all size sections). Bottom: instantaneous field of the net liquid-liquid mass source term

Finally, we give in figure 12 a qualitative comparison between experiments and numerical results for the instantaneous field. Figure 12a is an experimental visualization on the Mascotte test bench and figure 12b is an iso-surface (Y_l=0.95) of the LOx mass fraction in the CHARME solver.

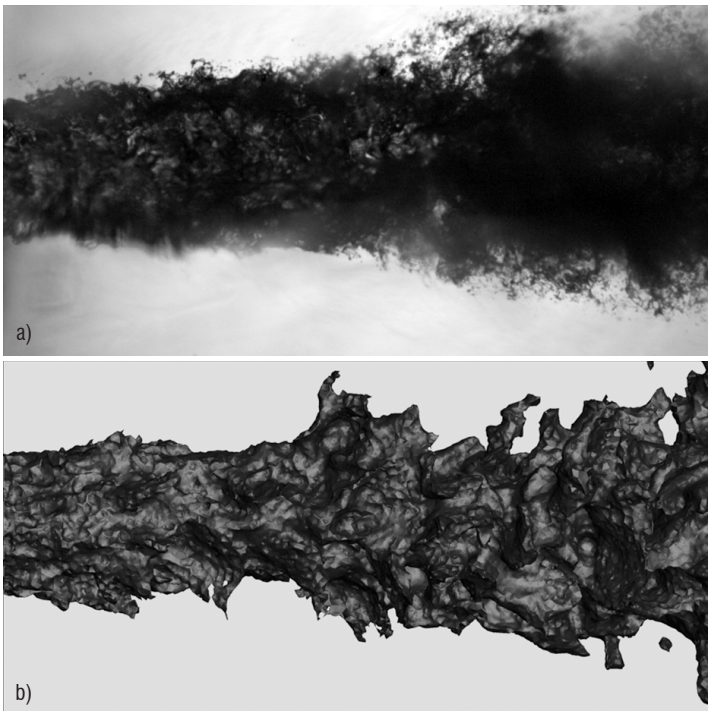

Figure 12 – Comparison between experiments and numerical results

Supercritical regime

For cryogenic engines running at high pressure, typically above 5 MPa, there is no phasic behavior between the cold injected oxygen and the warmer fluid where combustion phenomena occur. In this so-called supercritical regime, the lack of surface tension greatly modifies the mixing process, which does not involve droplet scattering as was the case in the subcritical regime. Oxygen dense core atomization is somewhat replaced by a peeling process, which strips off some oxygen dense clusters. These clusters are then rapidly stretched and heated, their surface to volume ratio not being minimized by interfacial energy consideration. The dense oxygen then undergoes a pseudo-boiling process, which is a continuous heating process from liquid-like dense states to gas-like thermodynamic states.

Fluid modeling

From a modeling point a view, supercritical regime thus appears at first sight as simpler than the subcritical regime, for neither scattered phase nor multiphasic bulk flow seem to be required. Some pressure laws, such as cubic equations of state (see BOX1), allow an analytic and continuous representation of supercritical fluids and one may think that a direct implementation of real gas thermodynamics in a standard CFD code would lead directly to a real gas capable code. This may be the case for DNS approaches [15], but more roughly discretized approaches such as LES or RANS need further development.

The reason for this lies in the fact that the width of the pseudo-boiling front results from a competition between heat conductivity and flow heterogeneities, such as stretch and turbulence. In rocket engine applications, the huge difference between the fuel injection speed leads to intense turbulence and thus to a pseudo-boiling front with a width of a few micrometers. Even with coarse front discretization, the number of points required to mesh one cubic centimeter of interest would be tremendous. Furthermore, with finite volume compressible approaches, the non-linearity of real gas thermodynamics in the pseudo-boiling region does not allow laxness in the front discretization, otherwise pressure oscillations are prone to appear.

Supercritical regime problems thus coincide with those encountered in the subcritical regime, that is to say, sharp interfacial or pseudo-interfacial phenomena that need to be discretized on coarse meshes. It is only natural that the way to handle it would also be similar.

A first approach is to spread the pseudo-boiling front over a sufficient number of discretization points using artificial diffusion [16]. This diffusion is triggered by a sensor allowing it to be active only in the pseudo-interfacial area and care must be taken to ensure that these extra terms in conservation equations do not themselves induce pressure oscillations. This could be achieved by adding compensatory energy source terms to nullify pressure variations.

Another approach consists in getting rid of thermodynamic non-linearity by means of a multi-fluid formulation. The pseudo-boiling interface is then no longer discretized, but rather distributed over the mesh cells where both fluids are present. This approach allows a sharper transition zone than the previous one for a given mesh, but requires additional conservation equations to be solved. The multi-fluid formulation is fundamentally a thermodynamic closure proposition for an averaged conservation equation in the way that it models subgrid structure complexity. Classical assumptions have indeed been shown [17] to fail, even with an LES filter size four time greater than the DNS grid size, and the proposed correction, based on pressure expansion in a Taylor series, is bound to fail for a greater LES filter size. The *a priori* distinction between the fluids can be interpreted as a Dirac delta based pdf in the thermodynamic space.

The simulations conducted at ONERA use a weakened multi-fluid approach, here dubbed a multi-phasic approach, enabling an easier implementation in the CFD code CEDRE created by ONERA. Indeed, if mass conservation equations are solved for each phase, only one total energy conservation equation is solved, the temperature of each "phase" being deduced from a mean temperature by means of *a priori* relations. These relations are designed in such a way that for the cold phase, the phase temperature corresponds to the mean temperature for low temperatures and smoothly reaches a maximal temperature T^c chosen below the pseudo-boiling temperature T^b for which the thermodynamical non-linearity is the greatest. Similarly, the hot phase temperature corresponds to the mean temperature for high temperatures and smoothly reaches a minimal temperature $T^h > T^b$ as the mean temperature decreases. This modification of the phase temperature can also be interpreted as a smooth prolongation of both phase thermodynamics before the non-linear zone is encountered, and thus as a smooth thermodynamic closure for the previously mentioned pdf. For the multi-phasic approach, only one global momentum equation is resolved, inducing equality of the phase velocities.

Mass exchange between the various phases is modeled as a volumic source term designed to relax in a given number of numerical time-steps the weight of the Dirac delta to a prescribed value depending on the mean temperature, so as to model pseudo-vaporization phenomena. This rather crude description of pseudo-interfacial phenomena, which only play a role in the one or two cell depth transition area where both phases are present, allows most of the thermodynamics non-linearity to be overcome in an energy-conservative way.

The small kinetic time scale for hydrogen combustion enables the use of a simplified combustion model based on relaxation toward a chemical equilibrium state in the hot phase. The time scale of this relaxation is linked to the turbulent time scale, in order to represent the limitation of combustion by the mixing phenomena.

Numerical simulation

Some LES have been performed on MASCOTTE test-bench configurations and yield satisfactory results concerning simulation stability. However, the fine representation of oxygen dense core breakup leads to the introduction and the coupling of time scales of rather different magnitude. Through developing Kelvin-Helmholtz instabilities, the oxygen dense core indeed breaks up into large dense clusters, which are slowly convected and pseudo-vaporized. The heterogeneity of dense core topology, especially its terminating clusters, greatly influences the flame, which rapidly adapts to it. A few dense core residence time must be waited in order to obtain the convergence of the mean dense core structure. The disparity of the time scales between the dense core and the hydrogen co-flow leads to the better representation of dense core breakup greatly increasing the cost of the simulation. This situation is worsened if one wishes to compute the entire MASCOTTE chamber. The rather slow motion of the burnt gases increases again to two fold the convergence time. As a consequence, the simulation presented here is not yet converged and only preliminary results are discussed.

Figure 13 shows a comparison between an experimental backlighting image [18] and an isodensity surface snapshot of the LES. As previously stated, the transition surface between cold dense oxygen and lighter hot gases is wrinkled by the co-flow, even if no small scale dense clusters are to be seen around the dense core. The numerical picture is taken just before a final breakup event as can be inferred from the shape of the isosurface, which displays a constricted shape near its end where separation will occur.

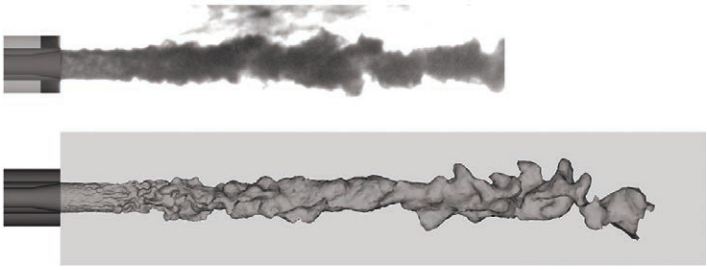

Figure 13 – Comparison between an experimental backlighting image of the A60 case [18] and a 200 kg/m^3 isodensity surface LES snapshot

The shape of the flame is shown in figure 14, in which a 1500 K isotemperature surface is drawn. This trumpet-like shape is the consequence of the flame being constrained by the backward-facing step toroidal recirculation vortex. Where the mean flow reattaches itself to the chamber boundary, the flame follows, leaving behind it a low velocity area, as already noted in similar configurations [19][20].

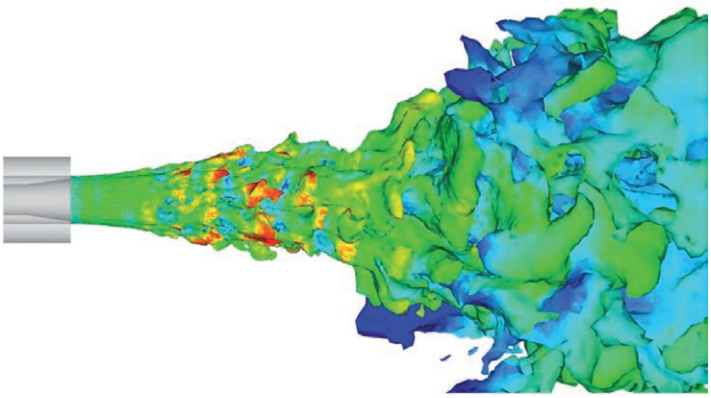

Figure 14 – 1500 K isotemperature surface LES snapshot

The comparison of the numerical results with the Abel transform of the OH* emission, which gives the position of the flame away, is performed in figure 15. The Abel transform from [21] is displayed at the bottom of this figure for reference. In the top picture, the far-from-being-converged mean OH production field is shown in pink over the reference picture and reasonable agreement is found between the experimental flame location and the numerical field.

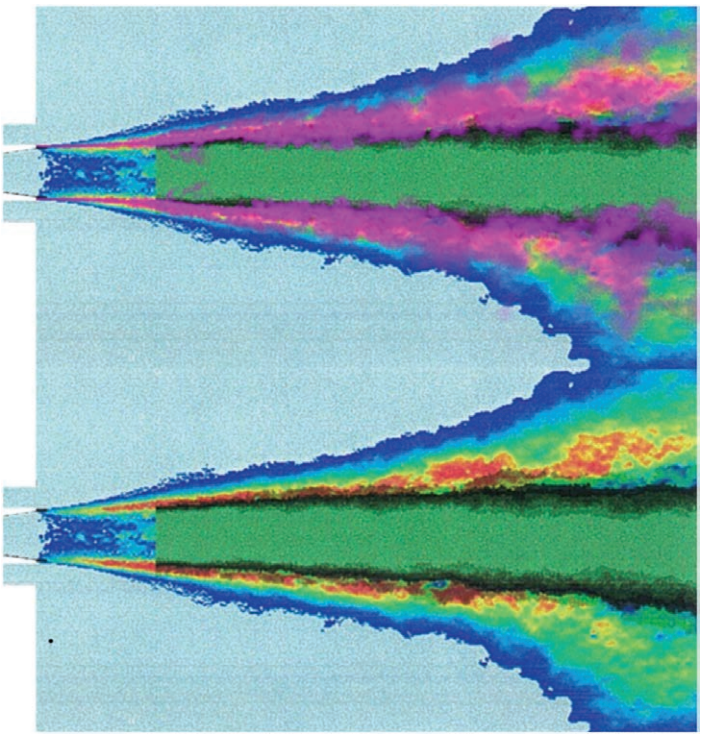

Figure 15 – Visualization of the comparison between experimental OH* [21] (up with computed mean OH production in pink)

Conclusion

Progress has been made in the modeling and simulation of physical phenomena at work in the field of cryogenic combustion.

A Large Eddy Simulation of the primary atomization in cryogenic combustion chamber has been performed by means of a fully Eulerian coupling strategy between a diffuse interface 4-equation (1-velocity) model and a kinetic based model, using specific numerical methods to ensure accuracy and robustness of the computation. The first results seem to be very promising, but need to be converged. For this reason, the comparisons with experiments are only qualitative at this moment. In the future, we intend to use a 7-equation (2-velocity) model, in order to improve the physical modeling of the primary atomization.

Supercritical oxygen dense core destabilization has been simulated with a specific dense to diluted transition model based on a weakened multi-fluid approach. As for the subcritical primary atomization case, the coupling between the different time scales and the need for a refined mesh to capture the pseudo interface topology lead to rather expensive simulation. In order to reduce the computational cost, pseudo interface modeling approaches are to be investigated ■

Box 1 - Cubic equation of state

Cubic equations of state have been obtained from the van der Waals equation of state [14] and can be written in the common form:

$$P = \left(\sum_{i=1}^{n_e} \frac{Y_i}{M_i} \right) \frac{RT}{v-b} - \frac{a(T)}{v^2 + uv + w}$$

where b stands for the covolume and $a(T)$ is an attraction parameter, which represents the effect of the London dispersion forces for molecules without permanent multipole moments. Further developments of the van der Waals equation of state led to various mixing rules used for the computation of the mixture covolume and attraction parameters from pure-species parameters, to various temperature dependencies of the attraction parameter $a(T)$ and to the introduction of the long range shape parameters u and w.

Pure species parameters are usually deduced from critical properties, in such a way that the cubic equation of state yields an exact pure-species critical point. Figure B1-1 shows the isothermal behavior of the cubic equation of state in a one-species case, the green square being the critical point of the represented species. For temperatures lower than the critical temperature, the phase equilibrium can be computed between a liquid phase and a gaseous phase, whereas above the critical temperature only a single-phase flow can occur. Despite their overall simplicity, which allows the analytic inversion of the pressure law thanks to Cardan's formulas, cubic equations of state reproduce reasonably well the fluid thermodynamic behavior and, as a consequence, they are often used in the field of CFD.

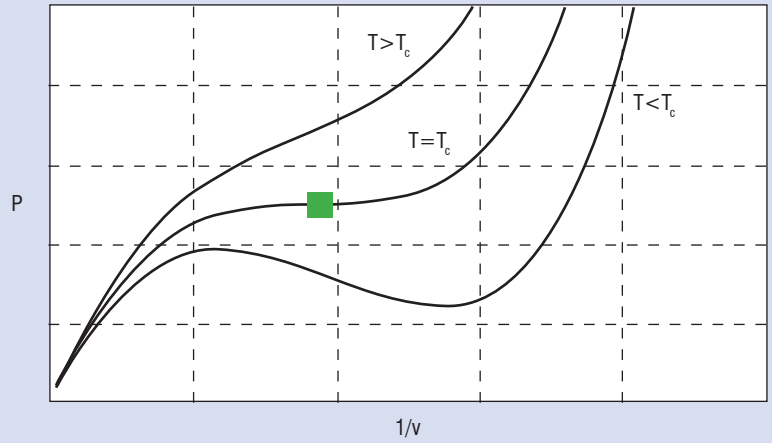

Figure B1-1 – Isothermal behavior of the cubic equation of state

References

[1] L. VINGERT, G. ORDONNEAU and P. GRENARD – *A Rocket Engine under a Magnifying Glass*. AerospaceLab Journal, Vol. 11, 2015.
[2] A. REFLOCH, B. COURBET, A. MURRONE, P. VILLEDIEU, C. LAURENT, P. GILBANK, J. TROYES, L. TESSE, G. CHAINERAY, J.B. DARGAUD, E. QUEMERAIS and F. VUILLOT – *CEDRE Software*. Aerospace Lab Journal, Issue 2, 2011.
[3] A. MURRONE and C. LE TOUZE – *Eulerian Coupling of Two-Phase Flow Models for the Large Eddy Simulation of the Atomization in Cryogenic Combustion Chamber*. 6th European Conference for Aeronautics and Space Sciences (EUCASS), Krakow, 2015.
[4] A. VALLET, A. BURLUKA and R. BORGHI – *Development of a Eulerian Model for the Atomization of a Liquid Jet*. Atomization and Sprays. 11:619–642, 2001.
[5] R. LEBAS, T. MENARD, P. A. BEAU, A. BERLEMONT and F.X. DEMOULIN – *Numerical Simulation of Primary Break-Up and Atomization : DNS and Modelling Study*. International Journal of Multiphase flow. 35:247–260, 2009.
[6] A. MURRONE and P. VILLEDIEU – *Numerical Modeling of Dispersed Two-Phase Flows*. AerospaceLab Journal, Issue 2, 2011.
[7] A. SIBRA – *Modélisation et étude de l'évaporation et de la combustion de gouttes dans les moteurs à propergol solide par une approche eulérienne Multi-Fluide*. PhD thesis, 2015.
[8] C. LE TOUZE – *Couplage entre modèles diphasiques à « phases séparées » et à « phase dispersée » pour la simulation de l'atomisation primaire en combustioncryotechnique*. PhD thesis, 2015.
[9] B. ABRAMZON and W.A. SIRIGNANO – *Droplet Vaporization Model for Spray Combustion Calculations*. International Journal of Heat and Mass Transfer, 32:160-16, 1989.
[10] K. POUGATCH, M. SALCUDEAN, E. CHAN and B. KNAPPER – *A Two-Fluid Model of Gas-Assisted Atomization Including Flow Through the Nozzle, Phase Inversion, and Spray Dispersion*. International Journal of Multiphase Flow, 35:7, 661–675, 2009.
[11] G. DUFOUR – *Modélisation multi-fluide eulérienne pour les écoulements diphasiques à inclusions dispersées*. PhD thesis, 2005.
[12] C. LE TOUZE, A. MURRONE and H. GUILLARD – *Multislope Muscl Method for General Unstructured Meshes*. Journal of Computational Physics, Vol. 284 , 2015, 389–418
[13] P. MARMOTTANT and E. VILLERMAUX – *On Spray Formation*. Journal of Fluid Mechanics, 498:73-112, 2004.
[14] J. D. VAN DER WAALS – *Over de Continuiteit van den Gas - en Vloeistoftoestand*. P.H.D thesis, Leiden, 1873.
[15] J. C. OEFELEIN – *Mixing and Combustion of Cryogenic Oxygen-Hydrogen Shear-Coaxial Jet Flames at Supercritical Pressure*. Combustion Science and Technology, Vol. 178, 2006.
[16] T. SCHMITT, L. SELLE, A. RUIZ and B. CUENOT – *Large-Eddy Simulation of Supercritical-Pressure Round Jets*. AIAA Journal, Vol. 48, 2010.
[17] L. C. SELLE, N. A. OKONG'O, J. BELLAN and K. G HARSTAD – *Modelling of Subgrid-Scale Phenomena in Supercritical Transitional Mixing Layers : an a priori Study*. Journal of Fluid Mechanics, Vol. 593, 2007.
[18] P. GICQUEL, M. BARAT and L. VINGERT – *Campagne de visualisation LOx sur le boîtier MASCOTTE à 6 MPa*. RT 1/06254 DEFA/DMTE, Nov. 2001.
[19] T. SCHMITT, Y. MERY, M. BOILEAU and S. CANDEL – *Large-Eddy Simulation of Oxygene/Methane Flames under Transcritical Conditions*. Proceedings of the Combustion Institute, Vol. 33, 2011.
[20] A. RUIZ – *Unsteady Numerical Simulations of Transcritical Turbulent Combustion in Liquid Rocket Engines*. P.H.D thesis, INP Toulouse 2012.
[21] S. CANDEL, M. JUNIPER, G. SINGLA, P. SCOUFLAIRE and C. ROLON – *Structure and Dynamics of Cryogenic Flames at Supercritical Pressure*. Combustion Science and Technology, Vol. 178, 2006.

AUTHORS

Pierre Gaillard is an engineer at MBDA, now working on ramjet and scramjet applications. He graduated from the Ecole Polytechnique and ISAE engineer schools in 2012 and received his PhD degree in mechanics from Université Paris 6 in 2015. His PhD work focused on supercritical flow and combustion.

Lionel Matuszewski is a research engineer at ONERA, working in the Liquid Propulsion Unit of the Fundamental and Applied Energetics Department (DEFA). He graduated from the Ecole Polytechnique and ISAE engineer schools in 2007. His research field is mainly focused on dense fluid modeling with application to supercritical combustion.

Clément Le Touze graduated from INSA de Rouen in 2011 with an engineering degree in propulsion and energetics, and received his PhD degree in applied mathematics from Université Nice Sophia Antipolis in 2015. He is now a research engineer in the Energetics department at ONERA. His main activities focus on the modeling and simulation of two-phase flows in the field of propulsion. He is also involved in the development of the CEDRE code, especially within the Eulerian SPIREE solver dedicated to dispersed two-phase flows.

Angelo Murrone graduated as an engineer from "Ecole Polytechnique Universitaire de Marseille" in 2000 and received a Ph.D. degree in Mechanics and Energetics from the University of Aix-Marseille I, France, in 2003. He has been working at ONERA since 2005 and his research concerns numerical modelling of multiphase flows and multi-physics simulations for Energetics and propulsion. He's currently head of the unit research in charge of the in-house multi-physics CEDRE code development.

Office National d'Études et de Recherches Aérospatiales
Chemin de la Hunière et des Joncherettes – BP 80100
91123 PALAISEAU Cedex
Tél. : +33 1 80 38 60 60 - Fax : +33 1 80 38 65 10
http://www.onera.fr